Science Advances
AAAS

advances.sciencemag.org/cgi/content/full/6/11/eaay1109/DC1

Supplementary Materials for

Protein modification with ISG15 blocks coxsackievirus pathology by antiviral and metabolic reprogramming

Meike Kespohl, Clara Bredow, Karin Klingel, Martin Voß, Anna Paeschke, Martin Zickler, Wolfgang Poller, Ziya Kaya, Johannes Eckstein, Henry Fechner, Joachim Spranger, Michael Fähling, Eva Katrin Wirth, Lilliana Radoshevich, Fabien Thery, Francis Impens, Nikolaus Berndt, Klaus-Peter Knobeloch, Antje Beling*

*Corresponding author. Email: antje.beling@charite.de

Published 11 March 2020, *Sci. Adv.* **6**, eaay1109 (2020)
DOI: 10.1126/sciadv.aay1109

The PDF file includes:

Other Supplementary Material for this manuscript includes the following:

(available at advances.sciencemag.org/cgi/content/full/6/11/eaay1109/DC1)

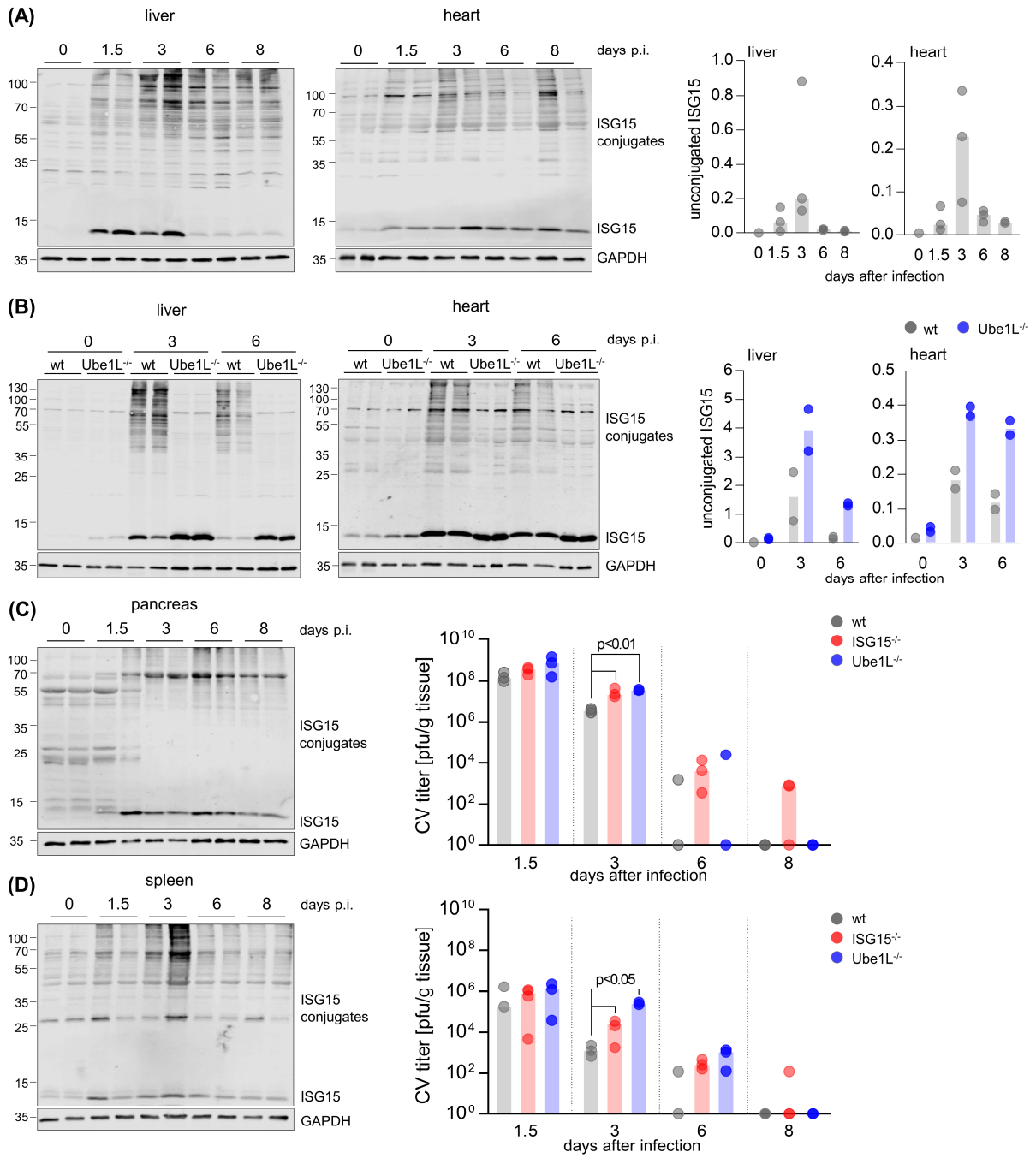

Fig. S1. CV-induced ISG15/ISGylation and its impact on virus load. Wild-type, ISG15$^{-/-}$ and Ube1L$^{-/-}$ mice were sacrificed at the indicated time periods after CV infection. (A) Tissue from liver and heart of wild-type mice was subjected to Western blot analysis using an ISG15-specific antibody. Each lane represents tissue homogenates obtained from a different animal. The levels of free ISG15 were quantified by densitometry and normalized to the GAPDH loading controls. Data of two to three individual mice per group are summarized as mean of relative ISG15 expression. (B) Tissue lysates were generated from liver (left) and heart (right) samples of wild-type and Ube1L$^{-/-}$ mice and expression levels of ISG15 were determined by Western blot analysis. The levels of free ISG15 were quantified by densitometry and normalized to the GAPDH loading controls. Data of two individual mice per group are summarized as mean relative ISG15 expression. Western blot analysis of pancreas (C) and spleen (D) lysates generated from CV infected wild-type mice. Infectious viral particles were quantified in pancreas (C) and spleen (D) obtained from wild-type, ISG15$^{-/-}$ and Ube1L$^{-/-}$ mice by plaque assay during CV infection. Each dot represents a different animal; data are summarized as the median values. Student's *t*-tests were conducted with *p*-values < 0.05 indicated in the graph.

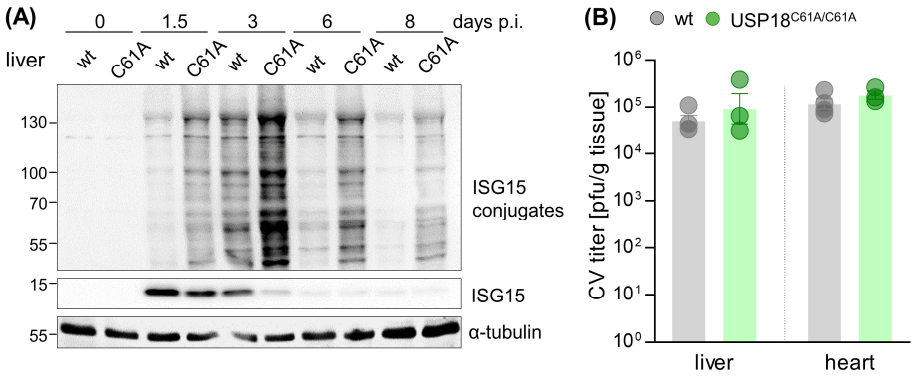

Fig. S2. Influence of USP18 inactivation in the early phase of CV infection. USP18C61A and wild-type littermate controls were infected with $1x10^5$ pfu CV. (A) Liver samples that were obtained at the indicated points in time were subjected to Western blot analysis using an ISG15-specific antibody. Each lane represents a tissue homogenate obtained from a different animal and is representative for three mice in each group. (B) Plaque assays were used to quantify infectious viral particles in the liver and heart at day three after infection. Each dot represents a different animal; data are summarized as mean ± SEM.

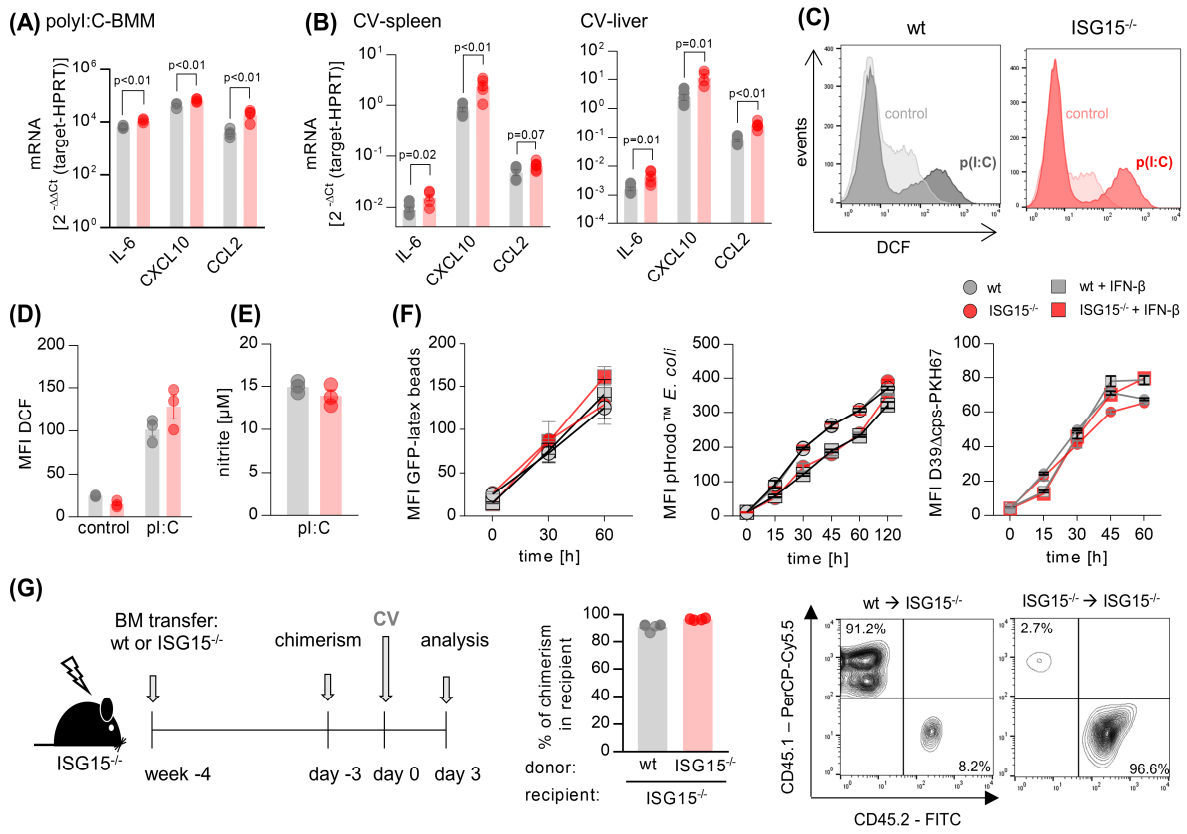

Fig. S3. Intact function of innate myeloid cells in ISG15$^{-/-}$ mice during CV infection. (A) BMM from wild-type and ISG15$^{-/-}$ mice were treated with 50 µg/ml poly(I:C) for 24 h. mRNA expression of the indicated genes was determined by TaqMan qPCR. One of three independent experiments is plotted. (B) ISG15$^{-/-}$ (n=6) and wild-type mice (n=5) were infected with 1x10^5 pfu of CV Nancy. Mice were sacrificed after three days and mRNA expression of the indicated cytokines and chemokines in spleen (left) and liver (right) were determined by TaqMan qPCR. (C+D) For the quantification of ROS in BMM, cells from wild-type and ISG15$^{-/-}$ mice were treated with poly(I:C) or left untreated (control), followed by incubation with DCFHDA for 1 h. Fluorescence signals were detected by flow cytometry. Representative histograms are shown. Data from one of three individual experiments is shown. (E) Similarly, the production of NO by BMM was induced by poly(I:C). Cell culture supernatants were subjected to colorimetric determination of nitrite, a stable metabolite of NO. Demonstrated data are representative for two independently performed experiments. (F) BMM from wild-type and ISG15$^{-/-}$ mice were incubated with IFN-β (100 U/ml, 12 h) or left untreated. Cells were loaded with GFP-labeled latex-beads, pHrodo™ *E. coli* particles or PKH67-labeled *S. pneumonia* (D39Δcps) as targets for phagocytosis and incubated at 37°C for the indicated points in time. Phagocytosis is represented as median fluorescence intensity (MFI) of the respective fluorophores determined by flow cytometry at the indicated points in time. Data are representative for three independently performed experiments. (G) Lethally irradiated ISG15$^{-/-}$ [CD45.2] mice were injected with either ISG15$^{-/-}$ [CD45.2] bone marrow or wild-type [CD45.1] bone marrow cells. Four weeks after transfer, peripheral blood cells were subjected to flow cytometry for analysis of CD45 expression. Representative flow cytometry plots are shown for each group. (A-G) Data are summarized as mean ± SEM; unpaired *t*-tests were performed revealing *p*-values < 0.05.

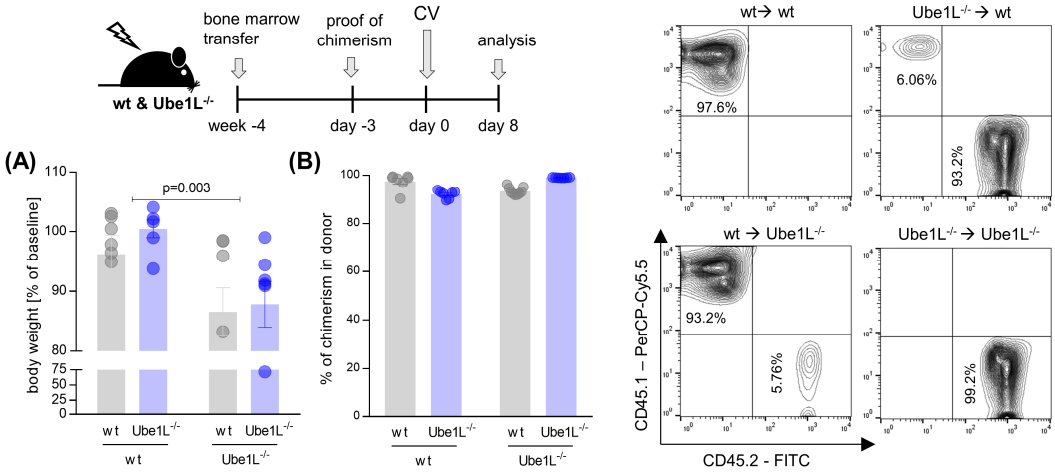

Fig. S4. Generation of Ube1L$^{-/-}$ bone marrow chimeric mice. Lethally irradiated wild-type mice [CD45.1] and Ube1L$^{-/-}$ mice [CD45.2] were reconstituted with bone marrow that was obtained from either wild-type [CD45.1] or from Ube1L$^{-/-}$ [CD45.2] mice. (A) Bars represent body weight change eight days after infection relative to the initial body weight (n=7 mice per group). Two-way ANOVA followed by post-hoc tests was performed. (B) Peripheral blood cells were analyzed by flow cytometry regarding the expression of CD45.1 and CD45.2. The percentage of donor cells with the respective recipients is depicted as mean ± SEM (left) and representative flow cytometry plots for each group are shown (right).

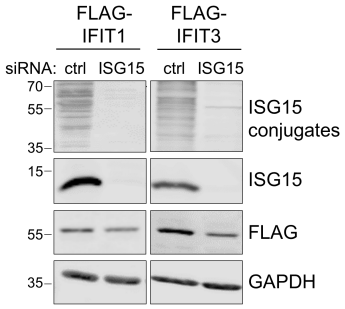

Fig. S5. Impact of ISG15 on IFIT1 and IFIT3 protein expression.
HeLa cells were transfected with either control or ISG15 specific siRNA before ISGylation was induced using 100 U/ml IFN-β. Transfection of FLAG-tagged IFIT1 or IFIT3 and analysis of IFIT1/3 expression levels after 24 h using a FLAG-tag specific antibody. Data are representative of three (IFIT1) or two (IFIT3) independently performed experiments.

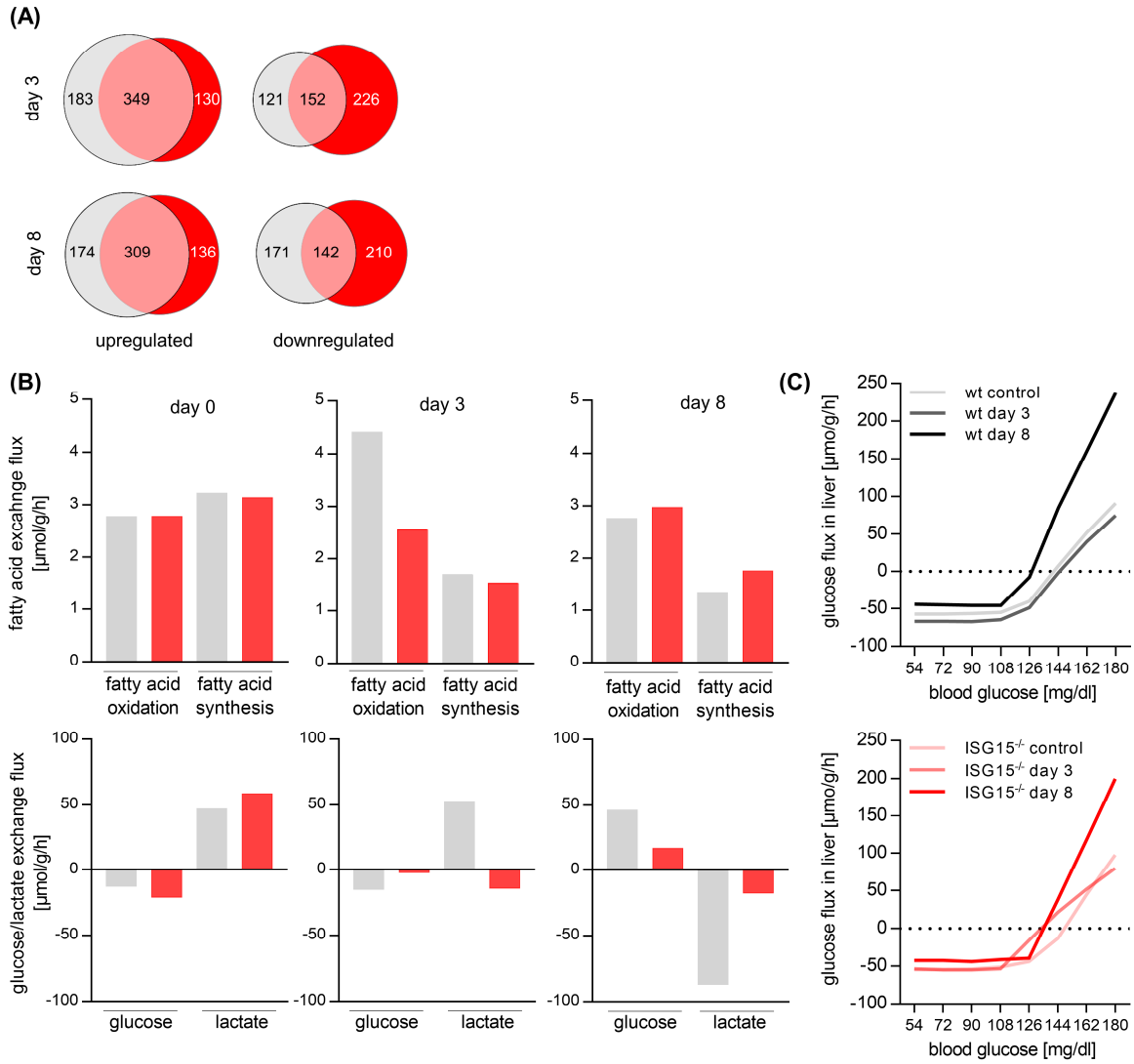

Fig. S6. Hepatic glucose flux in dependence of blood glucose.

Liver tissue was obtained from three different wild-type and ISG15$^{-/-}$ mice before as well as 3 and 8 days after CV infection. The proteome was analyzed by shot-gun proteomics. (A) Based on the hierarchical clustering depicted in Figure 5A, Venn diagrams were generated showing the number of unique proteins in the liver detected in wild-type and ISG15$^{-/-}$ mice at the indicated point in time. The respective number of identical proteins detected at the different states of CV infection in both wild-type and ISG15$^{-/-}$ mice is defined in the overlapping area. (B) Relative protein abundances were used to model central liver metabolism using HEPATOKIN1. Assuming a 24 h standard metabolite profile, glucose and lactate exchange fluxes as well as fatty acid (FA) oxidation and synthesis were computed and averaged over a diurnal period for wild-type and ISG15$^{-/-}$ mice at the indicated time points of infection. (C) For each disease state, the hepatic glucose exchange fluxes were simulated for the whole range of physiological blood glucose levels. Negative exchange fluxes indicate net release of glucose from the liver (gluconeogenesis) and positive values indicate hepatic glucose uptake (glycolysis).

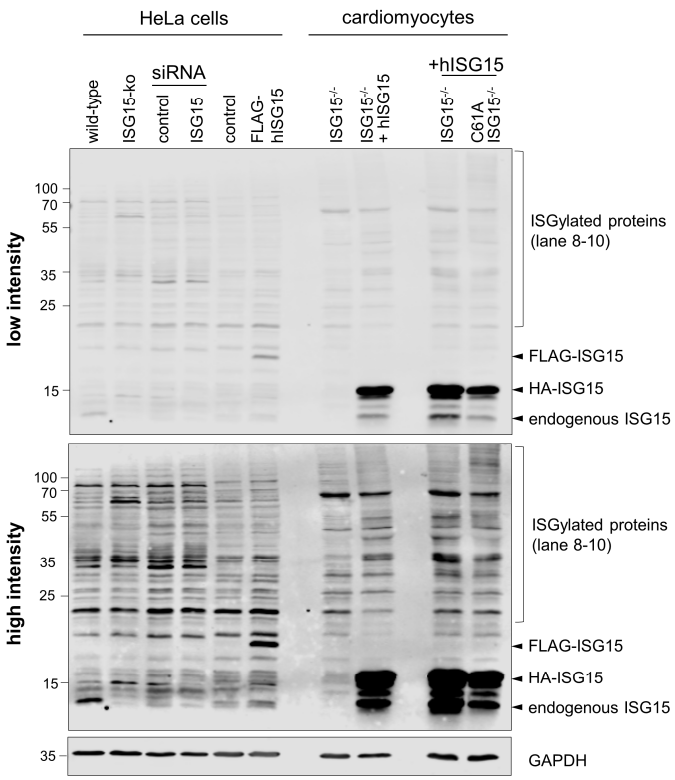

Fig. S7. Cell culture models to investigate the antiviral activity of human ISG15. ISG15-ko HeLa cells generated by CRISPR/Cas9-mediated gene editing (lane 2) and respective control cells (lane 1); HeLa transfected with siRNA targeting human ISG15 (lane 4) or a non-targeting control siRNA (lane 3); HeLa cells stably expressing FLAG-tagged human ISG15 (lane 6) and respective control cells (lane 5); ISG15$^{-/-}$ primary, murine cardiomyocytes transduced with AdV5-control (lane 7) or HA-tagged human ISG15 (MOI 25, 48 h, lane 8); ISG15$^{-/-}$ (lane 9) and ISG15$^{-/-}$USP18C61A primary, murine cardiomyocytes transduced with AdV5-HA-hISG15 (MOI 25, 48h, lane 10). Cell lysates were subjected to Western Blot analysis using an antibody targeting human ISG15. Low and high intensities are shown.

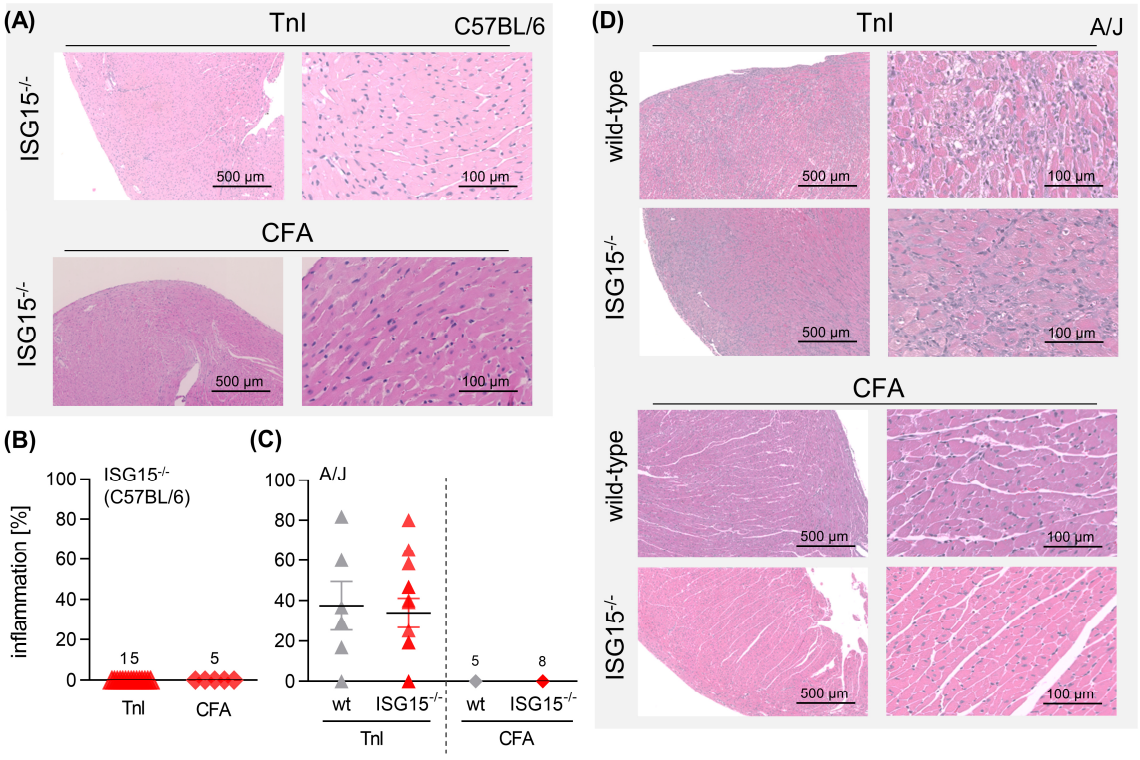

Fig. S8. Influence of ISG15 on experimental troponin I-induced autoimmune myocarditis. Since ISG15 controls loss of self-tolerance (27) and inflammatory cardiomyopathy triggered by viral infection also involves autoimmune disease processes (76), we questioned whether ISG15 is involved in the pathogenesis of autoimmune myocarditis (AM). Myocarditis was induced by troponin I peptide immunization (triangle) in ISG15$^{-/-}$ mice and respective wild-type littermate controls, either on a C57BL/6 (A+B) or an A/J (C+D) background. No-peptide control mice (diamonds) were treated with CFA only. Injections were repeated after 7 and 14 days. Mice were sacrificed after 28 days and heart tissue was subjected to histological analysis of inflammation. Ablation of ISG15 did not alter the inherent resistance of the C57BL/6 strain for development of AM (A+B). Similarly, the extent of inflammatory injury in heart tissue was not affected by ISG15 in A/J mice, which are susceptible to AM (C+D).

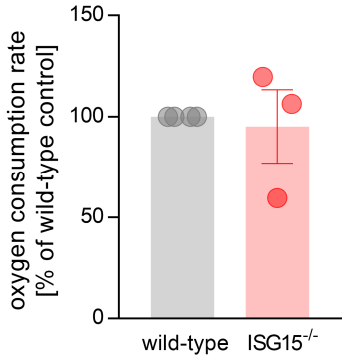

Fig. S9. Analysis of mitochondrial respiration in wild-type and ISG15$^{-/-}$ hepatocytes.
Primary hepatocytes were isolated from wild-type and ISG15$^{-/-}$ mice by liver perfusion with 0.3 mg/ml collagenase type I (Worthington Biochemical Co). Cells were filtered through a 70 µm cell strainer before they were applied to a Percoll gradient and centrifuged for 10 min at 50 rcf. 8x10^3 cells were seeded into a collagen-coated 96 well plate. Medium was changed to DMEM based assay medium with 2 mM glutamin and 2 mM glucose before the oxygen consumption rate was measured by an XFe 96well Extracellular Flux Analyzer. Data of three independent experiments was normalized to wild-type control and was summarized as mean ± SEM.